

Fairness Scheduling in User-Centric Cell-Free Massive MIMO Wireless Networks

Fabian Göttsch*, Noboru Osawa†, Issei Kanno†, Takeo Ohseki†, Giuseppe Caire*

Abstract

We consider a user-centric cell-free massive MIMO wireless network with L remote radio units, each with M antennas, serving K single-antenna user devices (UEs). Most of the current literature considers the regime $LM \gg K$, where the K UEs are active on each time-frequency slot, and evaluates the system performance in terms of *ergodic rates*. In this paper, we take a quite different viewpoint. We observe that the regime of $LM \gg K$ corresponds to a lightly loaded system with low sum spectral efficiency (SE). In contrast, in most relevant scenarios, the number of UEs is much larger than the total number of antennas (think of a sport event with $K \sim 10,000$ users and $ML \sim 200$ antennas), but users are not all active at the same time. To achieve high sum SE and handle $K \gg ML$, users must be scheduled over the time-frequency resource. The number of active users $K_{\text{act}} \leq K$ must be carefully chosen such that: 1) the network operates close to its maximum SE; 2) the active user set must be chosen dynamically over time in order to enforce fairness in terms of per-user time-averaged *throughput rates*. The fairness scheduling problem is canonically formulated as the maximization of a suitable concave componentwise non-decreasing *network utility function* of the per-user rates. Intermittent user activity imposes slot-by-slot coding/decoding which prevents the achievability of ergodic rates. Hence, we model the per-slot service rates using information outage probability. In order to obtain a tractable problem, we make a “decoupling” assumption on the CDF of the instantaneous mutual information seen at each UE k receiver. We approximately enforce this condition by introducing a conflict graph that prevents the simultaneous scheduling of users with large pilot contamination conflict and propose an adaptive scheme for instantaneous service rate scheduling based on locally estimating the mutual information CDF at each UE. Overall, the proposed dynamic scheduling is robust to system model uncertainties and can be easily implemented in practice.

Index Terms

User-centric, cell-free massive MIMO, fairness, scheduling, information outage probability.

*Technical University of Berlin, Germany. Emails: {fabian.goettsch, caire}@tu-berlin.de

†KDDI Research Inc., Japan. Emails: {nb-oosawa, is-kanno, ohseki}@kddi.com

I. INTRODUCTION

Multiuser Multiple-Input Multiple-Output (MU-MIMO) has been widely investigated from a theoretical viewpoint [1]–[4] and has become a cornerstone technology to achieve high spectral efficiency and serve a large number of user equipments (UEs) in both cellular [5]–[7] and local area wireless networks (see [8], [9] and references therein). Massive MIMO is a convenient implementation of MU-MIMO where the number of base station (BS) antennas M is much larger than the number of simultaneously served UEs [6], [10]. While massive MIMO was originally proposed for cell-based systems with per-BS processing [10]–[12], more recently the concept of cell-free user-centric networks has been promoted in order to provide a more uniform service to very densely packed users [7], [13]–[17]. In this paper we refer to the disaggregated reference model of 3GPP [18] (see Fig. 1) and consider a system formed by L radio units (RUs), each equipped with M antennas, connected to decentralized processing units (DUs) via a flexible fronthaul network. The RUs implement basic low-level PHY functions, such as FFTs/IFFTs for OFDM modulation, A/D and D/A conversion, and baseband/RF modulation/demodulation. The DUs implement the high-level PHY functions such as MIMO precoding/detection and coding/decoding of the individual user data streams. Higher layer functions such as user-centric cluster formation, pilot and power allocation, and dynamic scheduling, are implemented at a higher hierarchical level by one or more centralized units (CUs). We focus on *scalable* systems as defined in [7], [15], where each UE $k \in [K]^1$ is associated to a user-centric finite size set \mathcal{C}_k of RUs and each RU $\ell \in [L]$ serves a finite size set \mathcal{U}_ℓ of UEs.

A. Motivation

Early works on cell-free massive MIMO assumed $M = 1$ and $L > K$ [7, Ch. 2]. Recognizing that the placement of “more RUs than UEs” is hardly justifiable from an operator deployment cost viewpoint, more recent works have considered a more realistic RU/UE density regime $L < K < LM$ with $M > 1$ (e.g., see [7], [15]–[17], [19]). In these works, the K UEs are all simultaneously active and the system performance is studied in terms of the per-user *ergodic rates* (e.g., see [6], [7], [15]–[17]). However, the achievability of ergodic rates assumes that coding can be performed over a sufficiently large sequence of independent channel fading states, implying continuous transmission over many time-frequency slots. This assumption is incompatible with

¹We denote the set of the first positive N integers by $[N] = \{1, \dots, N\}$.

dynamic scheduling and per-slot coding/decoding, as well as with the “low latency” requirement, which is as a key feature of 5G [20], [21].

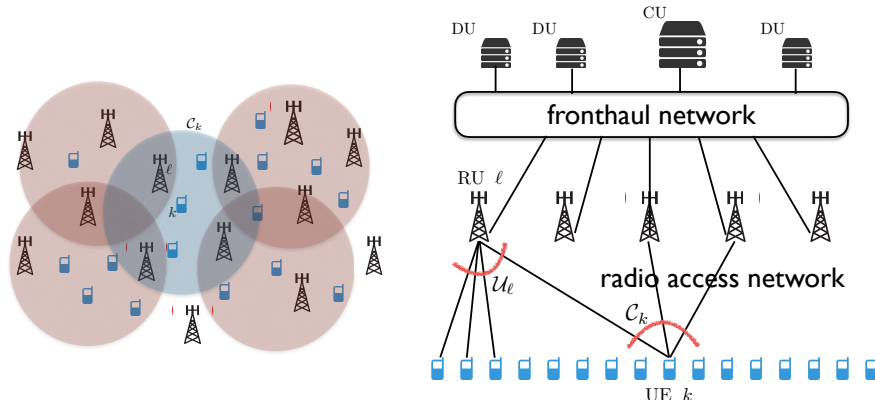


Fig. 1: Left: a sketch of the distributed cell-free user-centric network. Right: a sketch of the disaggregated network architecture. The cluster processors are hosted in the DUs. The CU hosts centralized (low complexity) processes, such as the user scheduler studied in this paper.

We claim that the regime $K < LM$ with continuous activity is not a practical regime of interest for such networks. Instead, a much more relevant regime is $K \gg LM$ where users must be scheduled over the time-frequency resource. Furthermore, we also claim that the per-user ergodic rate is not a significant performance metric in this scenario. Instead, the per-user (long-term average) *throughput rate* is a much more meaningful metric. In this sense, we must distinguish between the *instantaneous rate* scheduled to the $K_{\text{act}} < K$ active users on each given scheduling slot, and the *throughput rate* that each user accumulates as a time-average over a long sequence of slots. It is clear that some fairness criterion must be imposed such that all users get a chance to be scheduled over time and achieve a non-zero throughput rate, even though only a subset of active users is served with a positive instantaneous rate on each scheduling slot.

To motivate the problem, consider Fig. 2 (a), showing the total spectral efficiency (SE), i.e., the sum throughput rate, in bits per channel use (or bit/s/Hz) for the reference system described in Section V with $LM = 200$, where $L = 20$, $M = 10$, as a function of the number of users K , when all users are continuously active and encoding/decoding is done on blocks of $F = 10$ resource blocks (RBs) in frequency. We notice that for K much smaller than LM the SE is small and grows linearly with K . Interestingly, most of the current literature has focused on this *lightly loaded* regime of low total SE and relatively high per-user rates (see the corresponding cumulative distribution function (CDF) in Fig. 2 (b)). As K increases, the SE “flattens out” and reaches its peak. Near the maximum SE, the per-user throughput rates collapse (see the corresponding CDF in Fig. 2 (b)). If K keeps increasing, the SE slightly decreases, showing

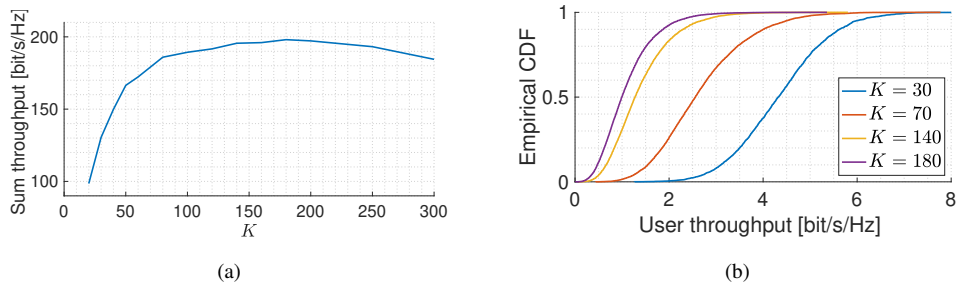


Fig. 2: Sum throughput rate and the empirical CDF of the user throughput rate for different K .

that in this regime the system becomes congested. Hence, a good scheduler should choose the number of active users K_{act} (slightly) on the left of the SE peak, i.e., at the end of the “linear regime” of SE vs. the number of active users. Beyond this point, a marginal increase of the SE is achieved at the cost of a large fraction of users with very small rate, which does not make sense from a practical service viewpoint. Extensive system simulation shows (see also our short conference version [22] of this work) that $K_{\text{act}} \approx \frac{LM}{2}$ is usually a good choice, and the exact number is a design parameter that depends on the level of frequency diversity F , and the desired tradeoff between sum SE and per-user throughput rate.

In order to gain intuition into the problem at hand, consider for example a system where the total bandwidth is partitioned into 100 frequency resource blocks (RBs) per time slot, serving a total number of 10,000 users with $L = 20$ RUs with $M = 10$ antennas each (e.g., see the real-world deployment in [23]). Every active user is allocated a block of $F = 10$ RBs in frequency to achieve a certain level of frequency diversity. Thus, the scheduler dynamically chooses on every slot a set of $K_{\text{act}} \approx \frac{LM}{2} = 100$ users out of 1,000 per RB in order to exploit the total system spatial degrees of freedom. The scheduler must also allocate an “instantaneous” rate to each active user since encoding/decoding is performed block by block, i.e., coding over a virtually infinite sequence of fading states is not possible. In this case, the instantaneous rate must be scheduled according to the notion of *information outage rate* (e.g., see [24]), where a non-vanishing block error probability is taken explicitly into account.

B. Novelty and contributions

In light of the above motivation, we study the fairness scheduling problem for a cell-free user-centric wireless network as defined in [7], [15]–[17]. We consider a full buffer model and canonically formulate fairness in terms of the maximization of a suitably defined network utility function, i.e., a concave componentwise non-decreasing function of the user throughput rates

[25]–[27]. In particular, we consider *proportional fairness* (PF) and *hard fairness* (HF), which are special cases of the family of so-called α -fairness utility functions [28].

The network utility maximization (NUM) problem is solved using the Lyapunov drift-plus-penalty (DPP) approach, which naturally yields a dynamic scheduling scheme [25]. However, the application of this general framework to our specific problem is non-trivial, because the instantaneous service rates, i.e., the rates scheduled to the active users, are random variables due to the finite diversity achieved in time and frequency (due to slot-by-slot coding) and in space (due to the limited number of spatial degrees of freedom which prevents massive MIMO “channel hardening” [29]). Scheduling with random instantaneous rates can be handled by using information outage probability as in [27]. This, however, requires the knowledge of the individual CDF of the mutual information at each user receiver, which in turn depends on the scheduling decision, i.e., of the selected set of active users.

In order to obtain a tractable problem, we make a critical “statistical decoupling” assumption: namely, that the CDF of the mutual information at each user k receiver depends only on the local channel statistics of UE k . This assumption holds true in the massive MIMO limit of $M \rightarrow \infty$ with constant K_{act}/M , under certain conditions on the channel statistics [27], [30], [31]. For systems with finite number of RU antennas M , the statistical decoupling assumption approximately holds when there is sufficient “self-averaging” of the interference term at the denominator of the *Signal to Interference plus Noise Ratio* (SINR) at each user decoder input. Intuitively, self-averaging holds when the multiuser interference is due to many small contributions. Hence, we enforce this condition by imposing that no two users causing strong mutual interference can be scheduled at the same time (this translates in a precise mathematical condition as seen later). To this purpose, we propose a novel *conflict graph* approach that prevents such “colliding” users to be scheduled together. Furthermore, since the mutual information CDF is intractable in closed form, we propose to adaptively estimate it at each UE k over a sliding window of past slots. The locally learned empirical CDF is used to schedule the instantaneous rate of the active users. Notice that rate adaptation based on the empirical statistics (e.g., RSSI, block error rate, etc.) collected over a sliding window of past slots is currently implemented in real systems. Thus, our approach can be seen as an information-theoretic version of such practical schemes.

The spread of the mutual information CDF is reduced as the frequency diversity order F increases. Our analysis can capture the effect of the finite frequency diversity order F on the overall system performance, unlike the ergodic rate analysis, where the finite diversity order

effect is completely lost. With the knowledge of the empirical mutual information CDF for each user, the scheduler solves at each slot a constrained maximization of the weighted sum outage rate, where the weights are recursively calculated as the backlogs of *virtual queues* and the constraint is expressed by the conflict graph. The problem takes the form of an integer linear program, which can be efficiently solved with standard tools even for fairly large systems.

We also notice that well-known problems such as pilot allocation and user-centric cluster formation have been treated in the current literature in the assumption that all users are active all the time [7], [16], [17], [19]. In contrast, in the presence of dynamic scheduling, an important question is whether pilot assignment and cluster formation should be performed *at each scheduling decision* (dynamic reassignment) or once for all to all users independently of the scheduling decisions (fixed assignment). Notice that the dynamic pilot assignment is supported by the current 5G NR standard, where the demodulation reference signal (DMRS) for channel estimation is associated with the physical uplink shared channel [5]. A fixed DMRS pilot assignment to users is not considered in the current 5G NR standard, but could be implemented in order to decrease the control signaling overhead. In this work, we compare the *reassignment* and the *fixed assignment* options in terms of their SE performance and show that a well-designed system with fixed assignment does not suffer large degradation with respect to the more complex and overhead-demanding reassignment.

C. Outline

In the next Section, we will describe the physical layer system model. Section III introduces the information outage rate and the fairness scheduling framework. The algorithmic solutions to approach the scheduling problem and practical aspects for implementation are presented in Section IV. Numerical results are shown in Section V.

II. PHYSICAL LAYER SYSTEM MODEL

In order to present the fairness scheduling problem and the proposed solution, we first need to review a rather standard cell-free user-centric system as described, with minor variations, in most literature (e.g., see [7], [13]–[17]). In particular, here we follow the notation of our previous work [17].

The system operates in TDD mode with L RUs, each equipped with M antennas, and K single-antenna UEs. Both RUs and UEs are distributed on a squared region on the 2-dimensional

plane. Without loss of generality, we focus on a system subband² formed by F frequency-domain RBs and assume the standard block fading model [10], for which each RB is formed by T time-frequency symbols over which the channel small-scale fading coefficients are constant and mutually independent for different RBs (in time and frequency) and different users. We let $\mathbb{H}(t, f) \in \mathbb{C}^{LM \times K}$ denote the overall channel matrix between all the K UE antennas and all the LM RU antennas on a given RB $f \in [F]$ in time slot t . The channel matrix is an $L \times K$ block matrix with $M \times 1$ blocks $\mathbf{h}_{\ell,k}(t, f) \sim \mathcal{CN}(\mathbf{0}, \mathbf{\Sigma}_{\ell,k})$, each representing the channel vector between the M antennas of RU ℓ and UE k .³ The random Gaussian vectors $\mathbf{h}_{\ell,k}(t, f)$ are i.i.d. over different t and f and mutually independent (but not identically distributed) for different ℓ and k . For later use, we let $\beta_{\ell,k} = \frac{1}{M} \text{tr}(\mathbf{\Sigma}_{\ell,k})$ denote the large-scale fading coefficient (LSFC), and $\mathbf{F}_{\ell,k}$ denote the tall unitary matrix spanning the channel dominant subspace, i.e., its columns are given by the (unit-norm) eigenvectors of $\mathbf{\Sigma}_{\ell,k}$ corresponding to the “largest” eigenvalues, as defined in [32] and made precise in Section V, where we consider a particular antenna correlation model.

In time slot t and for all RBs $f \in [F]$, each UE k is associated to its user-centric cluster $\mathcal{C}_k(t) \subseteq [L]$ of RUs. Consequently, each RU ℓ is associated to a set of UEs $\mathcal{U}_\ell(t) \subseteq [K]$. The UE-RU association is described by a bipartite graph $\mathcal{G}(t)$ (e.g., see Fig. 1), which may evolve in time depending on the association scheme. The graph has two classes of nodes (UEs and RUs) such that the neighborhood of UE-node k is $\mathcal{C}_k(t)$ and the neighborhood of RU-node ℓ is $\mathcal{U}_\ell(t)$. The set of edges of $\mathcal{G}(t)$ is denoted by $\mathcal{E}(t)$, i.e., $\mathcal{G}(t) = \mathcal{G}([L], [K], \mathcal{E}(t))$.

A. Channel State Information

For some given scheduling policy (to be specified later), we let $\mathcal{A}(t) \subseteq [K]$ denote the set of active users scheduled in slot t . At each time slot t , each RU ℓ obtains estimates $\hat{\mathbf{h}}_{\ell,k}(t, f)$ for all $k \in \mathcal{U}_\ell(t) \cap \mathcal{A}(t)$ and $f \in [F]$ from pilot sequences sent by the UEs in the UL. A codebook of τ_p *orthogonal* pilot sequences $\{\phi_j : j \in [\tau_p]\}$ is used for channel estimation. This requires that τ_p

²As in the example of Section I-A, K can be thought as the total number of users per subband. In general, the system bandwidth may be an integer multiple of such subband. Hence, the total number of users in the system is a corresponding integer multiple of K .

³Here, $\mathbf{0}$ indicates an all-zero vector of appropriate dimension and $\mathbf{\Sigma}_{\ell,k} = \mathbb{E}[\mathbf{h}_{\ell,k}(t, f)\mathbf{h}_{\ell,k}^H(t, f)]$ is the $M \times M$ covariance matrix. Notice that the statistics of the channel vectors are independent of time and frequency by the well-known widely adopted wide-sense stationary assumption [7], [15]–[17].

signal dimensions per block of T symbols are used for UL pilots, yielding a SE penalty factor $(1 - \frac{\tau_p}{T})$. Pilot sequences are normalized such that $\|\phi_j\|^2 = \tau_p \text{SNR}$ for all $j \in [\tau_p]$, where the parameter SNR denotes the average transmit energy per time-frequency symbol normalized to the thermal noise power spectral density N_0 . Each active user $k \in \mathcal{A}(t)$ is given a pilot index $p_k(t)$ and transmits sequence $\phi_{p_k(t)}$ over all F RBs in frequency. The UL pilot field received at RU ℓ on RB f in slot t is given by the $M \times \tau_p$ matrix $\mathbf{Y}_\ell^{\text{pilot}}(t, f) = \sum_{i \in \mathcal{A}(t)} \mathbf{h}_{\ell,i}(t, f) \phi_{p_i(t)}^H + \mathbf{Z}_\ell^{\text{pilot}}(t, f)$, where $\mathbf{Z}_\ell^{\text{pilot}}(t, f)$ is additive white Gaussian noise (AWGN) with elements i.i.d. $\sim \mathcal{CN}(0, 1)$.

For each UE $k \in \mathcal{U}_\ell(t) \cap \mathcal{A}(t)$, RU ℓ employs *pilot matching* (by right-multiplication of the pilot field by $\phi_{p_k(t)}$ and subspace projection on $\mathbf{F}_{\ell,k}$ to obtain the channel estimate [17]

$$\begin{aligned} \hat{\mathbf{h}}_{\ell,k}(t, f) &= \mathbf{F}_{\ell,k} \mathbf{F}_{\ell,k}^H \left(\frac{1}{\tau_p \text{SNR}} \mathbf{Y}_\ell^{\text{pilot}}(t, f) \phi_{p_k(t)} \right) \\ &= \mathbf{h}_{\ell,k}(t, f) + \mathbf{F}_{\ell,k} \mathbf{F}_{\ell,k}^H \left(\sum_{i \in \mathcal{A}(t) \setminus \{k\}: p_i(t) = p_k(t)} \mathbf{h}_{\ell,i}(t, f) \right) + \mathbf{F}_{\ell,k} \mathbf{F}_{\ell,k}^H \tilde{\mathbf{z}}_{p_k, \ell}(t, f), \end{aligned} \quad (1)$$

where $\tilde{\mathbf{z}}_{p_k, \ell}(t, f)$ is $M \times 1$ Gaussian i.i.d. with components $\mathcal{CN}(0, \frac{1}{\tau_p \text{SNR}})$ and where the second term of the sum in (1) is due to pilot contamination, i.e., it is the contribution of the active UEs sharing the same pilot as UE k . The covariance matrix of the pilot contamination term is given by $\Sigma_{\ell,k}^{\text{co}} = \sum_{i \in \mathcal{A}(t) \setminus \{k\}: p_i(t) = p_k(t)} \mathbf{F}_{\ell,k} \mathbf{F}_{\ell,k}^H \Sigma_{\ell,i} \mathbf{F}_{\ell,k} \mathbf{F}_{\ell,k}^H$. In particular, when $\mathbf{F}_{\ell,k}$ and $\mathbf{F}_{\ell,i}$ are nearly mutually orthogonal, i.e. $\mathbf{F}_{\ell,k}^H \mathbf{F}_{\ell,i} \approx \mathbf{0}$, the subspace projection is able to significantly reduce the pilot contamination effect [17]. In most of the concurrent literature [7], [15], [16], the channel statistics (in particular, the covariance matrices $\Sigma_{\ell,k}$) are assumed to be known. Schemes for channel subspace and covariance matrix estimation, respectively, in cell-free massive MIMO are presented in [17], [33]. In particular, the scheme in [17] is shown to achieve essentially the same performance of ideal channel subspace knowledge. Hence, for simplicity, in this work we assume that the subspace information $\mathbf{F}_{\ell,k}$ for all $\ell \in [L]$ and $k \in \mathcal{U}_\ell(t)$ is perfectly known, as justified by the results of [17].

For convenience, we denote by $\hat{\mathbb{H}}(t, f) \in \mathbb{C}^{LM \times K}$ the overall channel matrix estimated by the ensemble of the RUs. Notice that, beyond the estimation noise and pilot contamination, $\hat{\mathbb{H}}(t, f)$ differs from $\mathbb{H}(t, f)$ by the fact that it has an $M \times 1$ all-zero block for all positions (ℓ, k) such that $k \notin \mathcal{A}(t)$ or $k \notin \mathcal{U}_\ell(t)$. This captures the fact that RU ℓ can obtain a channel estimate $\hat{\mathbf{h}}_{\ell,k}(t, f)$ only if UE k is active (it is scheduled for transmission), and it is associated to RU ℓ . Hence, even in the absence of estimation noise and pilot contamination, the RUs have a partial view of the overall channel state [17].

B. Uplink Combining and Downlink Precoding

In this paper we consider the local linear MMSE detection and cluster-level combining scheme of [17], [34]. RU ℓ locally computes a UL receiver combining vector $\mathbf{v}_{\ell,k}(t, f)$ or each associated active UE $k \in \mathcal{U}_\ell(t) \cap \mathcal{A}(t)$ (see details in [17], [34]) based on the available channel estimates, i.e., the ℓ -th block row of $\hat{\mathbf{h}}_{\ell,k}(t, f)$. Using these local detection vectors, RU ℓ produces soft-output estimates of the time-frequency data symbols for each user $k \in \mathcal{U}_\ell(t) \cap \mathcal{A}(t)$. The estimated symbols of user k are sent via the fronthaul to the DU hosting the corresponding cluster processor. Such processor combines the signals from all RUs $\ell \in \mathcal{C}_k(t)$ to form the final received symbols for channel decoding. The cluster level combining coefficients, computed according to [17], [34], are denoted by $w_{\ell,k}(t, f)$. For convenience of notation, we define the $LM \times 1$ dimensional unit-norm overall combining vector for user k as $\mathbf{v}_k(t, f) = [w_{1,k}(t, f)\mathbf{v}_{1,k}^\top(t, f), w_{2,k}(t, f)\mathbf{v}_{2,k}^\top(t, f), \dots, w_{L,k}(t, f)\mathbf{v}_{L,k}^\top(t, f)]^\top$, where it is understood that $\mathbf{v}_{\ell,k}(t, f) = \mathbf{0}$ for all $\ell \notin \mathcal{C}_k(t)$.

In the DL, we use the same vectors $\mathbf{v}_k(t, f)$ as downlink precoders with equal power allocation for all active user data streams. The use of the UL combining vectors and DL precoding vectors is based on UL-DL duality, which holds approximately [17] or exactly [15], depending on which definition of achievable rate is used and the availability of channel and statistical information. In [35], we showed that using the UL combining vectors as DL precoding vectors with *uniform* power allocation over the DL data streams yields similar UL and DL rates. Hence, for the sake of simplicity, we use this method for the DL. We hasten to say that the scheduling approach developed in this paper can be applied to virtually any PHY and power allocation method, and the specific choice made here is for convenience of exposition.

C. Data Transmission and Instantaneous Mutual Information

In the UL, all active UEs transmit with the same average energy per symbol $P^{\text{ue}} = N_0\text{SNR}$. The received $LM \times 1$ symbol vector at the LM RU antennas for a single channel use on RB f in slot t of the UL is given by

$$\mathbf{y}(t, f) = \sqrt{\text{SNR}} \mathbb{H}(t, f)\mathbf{s}(t, f) + \mathbf{z}(t, f), \quad (2)$$

where $\mathbf{s}(t, f) \in \mathbb{C}^{K \times 1}$ is the vector of information symbols transmitted by the UEs on RB f in slot t (zero-mean unit variance and mutually independent random variables) and $\mathbf{z}(t, f)$ is an i.i.d. noise vector with components $\sim \mathcal{CN}(0, 1)$. The cluster processor of user k computes the estimate $\hat{s}_k(t, f) = \mathbf{v}_k(t, f)^\text{H} \mathbf{y}(t, f)$ of the time-frequency symbol $s_k(t, f)$ of user k . Letting

$\mathbb{H}(t) \triangleq \{\mathbb{H}(t, f) : f \in [F]\}$ and $\mathbb{v}_k(t) \triangleq \{\mathbb{v}_k(t, f) : f \in [F]\}$, the *instantaneous* mutual information between the transmitted symbol sequence $\{s_k(t, f) : f \in [F]\}$ and the detector soft-output sequence $\{\hat{s}_k(t, f) : f \in [F]\}$ in slot t (expressed in bits per time-frequency channel use, or bit/s/Hz) is a function of $\{\mathbb{v}_k(t), \mathbb{H}(t)\}$ and given by⁴

$$\mathcal{I}_k(\mathbb{v}_k(t), \mathbb{H}(t)) \triangleq \frac{1}{F} \sum_{f=1}^F \log(1 + \text{SINR}_k(t, f)), \quad (3)$$

where

$$\text{SINR}_k(t, f) = \frac{|\mathbb{v}_k(t, f)^H \mathbb{h}_k(t, f)|^2}{\text{SNR}^{-1} + \sum_{j \in \mathcal{A}(t): j \neq k} |\mathbb{v}_k(t, f)^H \mathbb{h}_j(t, f)|^2} \quad (4)$$

and \mathbb{h}_k is the k -th column of \mathbb{H} . In the DL, with suitable normalization, an active UE k receives

$$y_k^{\text{dl}}(t, f) = \mathbb{h}_k(t, f)^H \mathbb{x}(t, f) + z_k^{\text{dl}}(t, f), \quad (5)$$

where $z_k^{\text{dl}}(t, f) \sim \mathcal{CN}(0, \text{SNR}^{-1})$ and where $\mathbb{x}(t, f) = \sum_{k \in \mathcal{A}(t)} \mathbb{v}_k(t, f) s_k^{\text{dl}}(t, f)$ is the LM -dimensional vector of precoded symbols transmitted collectively by the RUs, with $s_k^{\text{dl}}(t, f)$ denoting the (unit-variance) information symbol sent to UE k at time slot t and RB f . The DL SINR of user k receiver is given by

$$\text{SINR}_k^{\text{dl}}(t, f) = \frac{|\mathbb{h}_k(t, f)^H \mathbb{v}_k(t, f)|^2}{\text{SNR}^{-1} + \sum_{j \in \mathcal{A}(t): j \neq k} |\mathbb{h}_k(t, f)^H \mathbb{v}_j(t, f)|^2}, \quad (6)$$

and the corresponding *instantaneous* mutual information is

$$\mathcal{I}_k^{\text{dl}}(\mathbb{V}(t), \mathbb{h}_k(t)) \triangleq \frac{1}{F} \sum_{f=1}^F \log(1 + \text{SINR}_k^{\text{dl}}(t, f)), \quad (7)$$

where we define the $ML \times K$ precoding matrix $\mathbb{V}(t, f)$ with columns $\mathbb{v}_k(t, f)$ (zero columns for inactive users), $\mathbb{V}(t) = \{\mathbb{V}(t, f) : f \in [F]\}$ and $\mathbb{h}_k(t) = \{\mathbb{h}_k(t, f) : f \in [F]\}$. Since the precoding vectors have unit norm, we have $\text{tr}(\mathbb{E}[\mathbb{x}(t, f)\mathbb{x}(t, f)^H]) = |\mathcal{A}(t)| = K_{\text{act}}$, where $|\cdot|$ denotes the cardinality of a set, i.e., the total transmit power in the UL and DL are both equal to $K_{\text{act}}P^{\text{ue}}$.

Remark 1. Expression (3) (resp., (7)) is referred to as “instantaneous” UL mutual information (resp., DL mutual information) because this is the mutual information between symbols $s_k(t, f)$ (resp, $s_k^{\text{dl}}(t, f)$) and the corresponding estimated symbols $\hat{s}_k(t, f)$ (resp., $y_k^{\text{dl}}(t, f)$) conditional on the specific realization of the (random) variables $\mathbb{v}_k(t), \mathbb{H}(t)$ (resp., $\mathbb{V}(t), \mathbb{h}_k(t)$). This term is

⁴This expression holds under the assumption that the user symbols are i.i.d. Gaussian and that the effective channel coefficients, i.e., the coefficients appearing in the numerator and denominator of the SINR expression in (4) are known at the receiver. Since these coefficients are constant over blocks of T symbols, for simplicity we make such assumption here. A more detailed analysis would consider the relation between block error probability and rate of random codes in the non-coherent block-fading channel with input $s_k(t, f)$ and output $\hat{s}_k(t, f)$, where coefficients are constant over F blocks of T symbol each. While this might be possible using the techniques in [36], [37], such information theoretic investigation goes well beyond the scope of this paper.

standard in the information theoretic literature on fading channels (e.g., see [24] and references therein), and should be distinguished from the standard conditional mutual information, which for the UL case would take the form

$$I(\{\hat{s}_k(t, f) : f \in [F]\}; \{s_k(t, f) : f \in [F]\} | \mathbf{v}_k(t), \mathbb{H}(t)) = \mathbb{E} \left[\frac{1}{F} \sum_{f=1}^F \log(1 + \text{SINR}_k(t, f)) \right]. \quad (8)$$

While (8) is a deterministic quantity that depends on the joint statistics of the true and estimated channels $\{\mathbb{H}(t, f), \hat{\mathbb{H}}(t, f) : f \in [F]\}$, (3) and (7) are random variables, functions of the (random) instantaneous realization of $\{\mathbb{H}(t, f), \hat{\mathbb{H}}(t, f) : f \in [F]\}$. \diamond

III. FAIRNESS SCHEDULING

For convenience of exposition, we shall illustrate the scheduling problem for the UL (the application to the DL follows immediately). At each scheduling slot t , a scheduling policy must: 1) select a set of active users $\mathcal{A}(t)$; 2) select the coding rates $\mathbf{r}(t) = \{r_k(t) : k \in \mathcal{A}(t)\}$ at which these users transmit their information. The system state in our case is $\{\mathbb{H}(t)\}$, a stationary and ergodic matrix-valued Gaussian process as described in Section II. A stationary scheduling policy γ is a time-invariant function $\gamma : \mathbb{H}(t) \mapsto \{\mathcal{A}(t), \mathbf{r}(t)\}$ [25]. We denote by Γ the set of all feasible stationary policies for the system at hand, i.e., compliant with the PHY layer channel estimation, receiver/precoding vector calculation and Gaussian coding described in Section II. In particular, driven by the discussion in Section I-A and exemplified by Fig. 2, we focus on the case where K may be very large, and we consider policies operating in the “good” load regime such that $|\mathcal{A}(t)| \leq K_{\text{act}}$, where the maximum number of active users K_{act} is chosen to strike a good tradeoff between total system SE and per-user rates. In order to proceed, we introduce the following two key assumptions:

A1: The rate allocation $r_k(t)$ to active user k on slot t is a function of the channel statistics but not of the instantaneous realization of $\{\mathbf{v}_k(t), \mathbb{H}(t)\}$, which is known causally. \diamond

A2: For any user $k \in \mathcal{A}(t)$, the complementary CDF of the instantaneous mutual information

$$P_k(r) \triangleq \mathbb{P}(\mathcal{I}_k(\mathbf{v}_k(t), \mathbb{H}(t)) > r) \quad (9)$$

is independent of the active user set $\mathcal{A}(t)$ but only on its size $K_{\text{act}} = |\mathcal{A}(t)|$. \diamond

Remark 2. Assumption A1 reflects the common practice in rate allocation in real-world systems [38], [39], where users are instructed to transmit a given Modulation and Coding Scheme (MCS) in a family spanning a wide range of coding rates on the basis of some “local” statistics accumulated in a time sliding window (e.g., RSSI, block error probability, in the past few time

slots). The sliding window approach is used to track statistical changes, e.g., a user moving from a position close to a RU to a position farther away. This prevents slot by slot rate adaptation depending on the instantaneous realization of the channel small scale fading states, which would be too fast to track and too demanding in terms of protocol overhead, to signal to the receiver the used MCS. In practice (see Section IV), since the analytical characterization of $P_k(r)$ is intractable, the scheduler uses empirical statistics collected over a window of time slots.

Assumption A2 is motivated by the fact that, for a large system with many randomly distributed UEs and RUs, the cumulative interference effect of all other active users on a given active user k is approximately “self-averaging” and is weakly dependent on which individual active users are selected. This assumption is verified exactly in certain limiting conditions and symmetric situations as for example in massive MIMO multicell-networks (e.g., see [10]–[12], [31]). For the system at hand, A2 holds only approximately, provided that UEs with strong mutual pilot contamination are not scheduled together [22]. For the sake of problem tractability, we shall develop our scheduling scheme under A2, and introduce a conflict graph constraint in the active user selection problem such that A2 is effectively (approximately) satisfied. \diamond

A. Service Rate, Throughput Region, and Network Utility Maximization

As already mentioned, because of the discontinuous user activity due to scheduling, coding over a long sequence of scheduling slots is impossible or impractical.⁵ With block-by-block coding/decoding, each codeword spans a single channel state $\mathbb{H}(t)$. In this case, the block error rate of optimal codes for the effective Gaussian channel with input $s_k(t, f)$ and output $\hat{s}_k(t, f)$ as defined in Section II-C is well approximated by the so-called *information outage probability*, i.e., the probability that the instantaneous mutual information is less than the coding rate [24], [27]. We define the instantaneous *service rate* $\mu_k(t)$ of user k as the number of information bits per s/Hz (i.e., normalized by the block length TF in channel uses) that are effectively delivered to the receiver in slot t . This is given by

$$\mu_k(t) = \begin{cases} (1 - \frac{\tau_p}{T})R_k(t), & \text{if } k \in \mathcal{A}(t), \\ 0, & \text{if } k \notin \mathcal{A}(t), \end{cases} \quad (10)$$

⁵In particular, this is in conflict with the low latency requirements typical of 5G systems [20], [21].

where we define the random variable $R_k(t) \triangleq r_k(t) \times \mathbb{1}\{\mathcal{I}_k(\mathbb{V}_k(t), \mathbb{H}(t)) > r_k(t)\}$, and where $\mathbb{1}\{\mathcal{S}\}$ is the indicator function of an event \mathcal{S} . For a given stationary policy $\gamma \in \Gamma$, the per-user *throughput rate* is the long-term time-averaged service rate, i.e.,

$$\bar{\mu}_k = \lim_{t \rightarrow \infty} \frac{1}{t} \sum_{\tau=0}^{t-1} \mu_k(\tau) = \mathbb{E}[\mu_k(\mathbb{H}, \gamma)], \quad (11)$$

where \mathbb{H} has the same marginal statistics of $\mathbb{H}(t)$ and $\mu_k(\mathbb{H}, \gamma)$ has the same marginal statistics of $\mu_k(t)$ in (10). The converge of the time average to the ensemble expectation in (11) is with probability 1 due to the stationarity and ergodicity of the channel state and the stationarity of the scheduling policy [25].

A throughput rate vector $\bar{\boldsymbol{\mu}} = [\bar{\mu}_1, \dots, \bar{\mu}_K]^T$ is feasible if there exists a scheduling policy $\gamma \in \Gamma$ such that $\bar{\mu}_k \leq \mathbb{E}[\mu_k(\mathbb{H}, \gamma)]$ for all $k \in [K]$. Hence, the system throughput region is [25]

$$\mathcal{R} = \text{coh} \bigcup_{\gamma \in \Gamma} \left\{ \bar{\boldsymbol{\mu}} \in \mathbb{R}_+^K : \bar{\mu}_k \leq \mathbb{E}[\mu_k(\mathbb{H}, \gamma)], \forall k \right\}, \quad (12)$$

where ‘‘coh’’ denotes the closure of the convex hull. Two important properties of \mathcal{R} are [25]:

- 1) Queue stability region: given the system at hand, consider stationary and ergodic *exogenous* traffic arrival processes $\{A_k(t) : k \in [K]\}$, such that $A_k(t)$ is the number of information bits per s/Hz arriving at the transmitter of UE k in slot t , with arrival rates $\lambda_k = \mathbb{E}[A_k(t)]$. Let each UE k have a transmission queue $Q_k(t)$ that evolves according to the standard dynamic equation $Q_k(t+1) = [Q_k(t) - \mu_k(t)]_+ + A_k(t)$, where for any $x \in \mathbb{R}$ we define $[x]_+ := \max\{x, 0\}$. An arrival rate vector $\boldsymbol{\lambda} = (\lambda_1, \dots, \lambda_k) \in \mathcal{R}$ can be stabilized, i.e., there exists a stationary scheduling policy for which all system queues are *strongly stable* [25], if and only if there exists a strictly non-negative vector $\boldsymbol{\epsilon}$ for which $\boldsymbol{\lambda} + \boldsymbol{\epsilon} \in \mathcal{R}$.
- 2) Sufficiency of stationary policies: \mathcal{R} cannot be enlarged by non-stationary policies.

In this paper, we are concerned with scheduling for fairness, rather than scheduling for queue stability. In this case, we consider the ‘‘infinite buffer’’ model where each UE is provided with an infinite buffer of data to transmit. Rather than stabilizing transmission queues for random exogenous arrival processes, we wish to operate the system such that each user has its own ‘‘fair share’’ of the overall throughput. The problem is canonically formalized as a NUM as follows.

Definition 1. NUM Problem. Let $g(\cdot)$ denote a concave entry-wise non-decreasing function of per-user throughput rates $\bar{\boldsymbol{\mu}}$, whose shape (concavity) captures a desired notion of fairness. The fairness scheduling problem consists of finding the scheduling policy solution of the NUM:

$$\text{maximize } g(\bar{\boldsymbol{\mu}}), \quad \text{subject to } \bar{\boldsymbol{\mu}} \in \mathcal{R}. \quad (13)$$

◇

Since \mathcal{R} is convex and compact, the solution of (13) always exists and it is at some point on the Pareto boundary of \mathcal{R} . Letting $\bar{\boldsymbol{\mu}}^*$ denote such solution, there exists a scheduling policy γ^* that achieves $\bar{\boldsymbol{\mu}}^*$. Finding γ^* by directly solving (13) is generally impractical. In fact, despite (13) is a convex optimization problem, the constraint region \mathcal{R} is not generally characterized by a finite number of linear inequalities. Fortunately, the NUM problem (13) can be solved to any desired degree of accuracy in an algorithmic way by using the *Lyapunov DPP* framework of [25]. Instead of looking for a stationary policy, the DPP approach constructs a *dynamic policy* that yields a long-term average throughput point arbitrarily close to the optimum $\bar{\boldsymbol{\mu}}^*$ under mild conditions (see the assumptions in Theorem 1). The next section develops such an algorithmic solution for the problem at hand.

B. Dynamic Scheduling Policy

We start with the following somehow obvious lemma:

Lemma 1. Outage Rate Allocation. For each $k \in [K]$ define

$$r_k^* = \operatorname{argmax}_{r \geq 0} r P_k(r). \quad (14)$$

and for a given active user set $\mathcal{A}(t)$ define the vector $\mathbf{r}^*(t)$ with k -th component equal to r_k^* if $k \in \mathcal{A}(t)$ and zero otherwise. For any stationary policy $\gamma : \mathbb{H}(t) \mapsto (\mathcal{A}(t), \mathbf{r}(t))$ yielding the throughput rate vector $\bar{\boldsymbol{\mu}}(\gamma)$, the stationary policy γ^* that coincides with γ on the active user set $\mathcal{A}(t)$ but uses rates $\mathbf{r}^*(t)$ in (14) yields $\bar{\boldsymbol{\mu}}(\gamma^*) \geq \bar{\boldsymbol{\mu}}(\gamma)$, where the inequality holds componentwise (not necessarily strictly). □

Proof: The throughput rate of user k under γ is given by

$$\begin{aligned} \bar{\mu}_k(\gamma) &= \left(1 - \frac{\tau_p}{T}\right) \mathbb{E} [r_k(t) \mathbb{1} \{\mathcal{I}_k(\mathbb{v}_k(t), \mathbb{H}(t)) > r_k(t)\} \mathbb{1} \{k \in \mathcal{A}(t)\}] \\ &= \left(1 - \frac{\tau_p}{T}\right) r_k(t) P_k(r_k(t)) \mathbb{P}(k \in \mathcal{A}(t)), \end{aligned} \quad (15)$$

where (15) follows from the fact that the distribution of $\mathcal{I}_k(\mathbb{v}_k(t), \mathbb{H}(t))$ does not depend on $\mathcal{A}(t)$ (Assumption A2). Since γ and γ^* coincide in $\mathcal{A}(t)$ and differ only in the rate allocation, replacing $r_k(t)$ with r_k^* in (15) maximizes the throughput rate. ■

Lemma 1 solves the outage rate allocation problem in the sense that we can restrict to policies that use the coding rate r_k^* in (14) for all active users. Next, using the theory in [25], [27], we are

ready to state the dynamic scheduling policy and prove its properties under assumptions A1 and A2. We associate to each UE $k \in [K]$ a virtual queue $Q_k(t)$. This queue does not represent bits that arrive at UE k transmitter and wait to be delivered to the receiver, since our system has full buffer and no random arrival. Instead, the values $\{Q_k(t) : k \in [K]\}$ are iteratively computed and yield the weights for a weighted sum rate maximization (WSRM) problem that the scheduler solves at every slot t to determine the set of active users. The queues can be initialized as $Q_k(0) = 0$ for all k .

Definition 2. Fairness dynamic scheduling. *Let $V > 0$, $A_{\max} > 0$ and $K_{\text{act}} \geq 1$ be the parameters of the scheduling policy. For each $t = 0, 1, 2, \dots$, the policy $\hat{\gamma}$ iterates the following steps:*

- 1) *Virtual arrivals: let $A_k(t) = a_k$, where $\mathbf{a} = [a_1 \dots a_K]^\top$ is the solution of the convex optimization problem*

$$\text{maximize } Vg(\mathbf{a}) - \sum_{k \in [K]} a_k Q_k(t), \quad \text{subject to } \mathbf{a} \in [0, A_{\max}]^K \quad (16)$$

- 2) *User selection via WSRM: let $\mathcal{A}(t)$ be the solution of*

$$\text{maximize } \sum_{k \in \mathcal{A}} Q_k(t) r_k^* P_k(r_k^*), \quad \text{subject to } \mathcal{A} \subseteq [K], \quad |\mathcal{A}| \leq K_{\text{act}} \quad (17)$$

- 3) *Transmission: each user $k \in \mathcal{A}(t)$ transmits with rate r_k^* . The cluster receivers compute the receiving vectors from the estimated channels in $\hat{\mathbb{H}}(t)$ and attempt decoding. Let $\mu_k(t)$ denote the resulting service rate (see (10)).*

- 4) *Virtual queue update: for all $k \in [K]$ compute the new virtual backlog value as*

$$Q_k(t+1) = [Q_k(t) - \mu_k(t)]_+ + A_k(t). \quad (18)$$

◇

The following result establishes the performance guarantee of scheduling policy $\hat{\gamma}$.

Theorem 1. *Suppose that channel states \mathbb{H} are i.i.d. over timeslots. Under assumptions A1 and A2, we consider the scheduling policy $\hat{\gamma}$ from Definition 2 and constants $V > 0$, $A_{\max} > 0$. We further assume that there exists a point $\mathbf{r} \in \mathcal{R}$ with strictly positive entries such that $g(\mathbf{r}/2) > -\infty$. Then:*

- a) *The utility associated with the time average transmission rates achieved by $\hat{\gamma}$ satisfies*

$$\liminf_{t \rightarrow \infty} g\left(\frac{1}{t} \sum_{\tau=0}^{t-1} \mathbb{E}[\boldsymbol{\mu}(\tau)]\right) \geq g(\bar{\boldsymbol{\mu}}^*(A_{\max})) - \frac{C}{V}, \quad (19)$$

where

$$C \triangleq \frac{K}{2} \left(A_{\max}^2 + \mathbb{E} \left[\left(\frac{1}{F} \sum_{f=1}^F \log \left(1 + \frac{|\mathbb{h}_{k^*}(t, f)|^2}{\text{SNR}^{-1}} \right) \right)^2 \right] \right) \quad (20)$$

with $k^* = \arg \max_{k \in [K]} \frac{1}{F} \sum_{f=1}^F \log \left(1 + \frac{|\mathbb{h}_k(t, f)|^2}{\text{SNR}^{-1}} \right)$, and where $\bar{\boldsymbol{\mu}}^*(A_{\max})$ is the solution of problem (13) with the additional constraint $0 \leq \bar{\mu}_k \leq A_{\max}$ for all $k \in [K]$.

b) For any point $\bar{\boldsymbol{\mu}} \in \mathcal{R}$ such that $0 \leq \bar{\mu}_k \leq A_{\max}$ for all k , and for any value $\beta \in [0, 1]$ we have

$$\limsup_{t \rightarrow \infty} \frac{1}{t} \sum_{\tau=0}^{t-1} \sum_{k=1}^K \bar{\mu}_k \mathbb{E}[Q_k(\tau)] \leq \frac{C + V [g(\bar{\boldsymbol{\mu}}^*(A_{\max})) - g(\beta \bar{\boldsymbol{\mu}})]}{1 - \beta}. \quad (21)$$

Hence, all the virtual queues $Q_k(t)$ are strongly stable (see definition in [25]).

Proof: See Appendix A. ■

Theorem 1 implies that if A_{\max} is sufficiently large, such that $A_{\max} \geq \bar{\mu}_k^*$ for all k , then $\liminf_{t \rightarrow \infty} g \left(\frac{1}{t} \sum_{\tau=0}^{t-1} \mathbb{E}[\boldsymbol{\mu}(\tau)] \right) \geq g(\bar{\boldsymbol{\mu}}^*) - \frac{C}{V}$. Hence, by choosing a sufficiently large V , $\hat{\gamma}$ can approach $g(\bar{\boldsymbol{\mu}}^*)$ as closely as desired with convergence time that scales as $O(V)$ due to (21).

IV. ALGORITHMIC AND PRACTICAL ASPECTS

As in the previous section, we focus on the UL. The algorithms can easily be applied to the DL case by using the DL instantaneous mutual information (7) and its CDF in place of its UL counterpart. For assumption A2 to hold, we need to guarantee that the pilot contamination affecting UE k is negligible. In fact, a strong pilot contamination severely affects the quality of the channel estimates (1) and this affects both the useful signal term and the interference term in the SINR expression (4). Severe pilot contamination occurs if users $k, k' \in \mathcal{A}(t)$ share at least one RU in their user-centric cluster, have the same UL pilot, and their channel subspaces with respect to the shared RUs are strongly aligned, i.e., far from mutually orthogonal.

We propose to prevent strong pilot contamination between active users by introducing a conflict graph that constrains the scheduling decisions. Note that it is generally not advisable to schedule users with strong mutual interference. Hence, although this is a heuristic approach, it is expected that the conflict graph does not limit significantly the space of *good policies*. Interestingly, by introducing the conflict graph as a constraint in the general WSRM (17), the problem becomes a linear integer program.

In particular, we define the conflict graph $\mathcal{C} = ([K], \mathcal{E}_c)$ with a vertex set corresponding to all K UEs in the network and an edge set \mathcal{E}_c accounting for the conflicts. A UE-pair (k, k') is

in conflict if the following three conditions are satisfied:

- 1) the UEs are associated to at least one common RU, i.e., $\mathcal{C}_{k,k'} \triangleq \mathcal{C}_k \cap \mathcal{C}_{k'} \neq \emptyset$;
- 2) the UEs are assigned the same UL pilot, i.e., $p_k = p_{k'}$;
- 3) the channels of the UEs with respect to at least one RU $\ell \in \mathcal{C}_{k,k'}$ are strongly aligned, i.e.,

$$\|\mathbf{F}_{\ell,k}^H \mathbf{F}_{\ell,k'}\|_F > \eta_{\mathbf{F}}, \quad \text{for some } \ell \in \mathcal{C}_{k,k'}, \quad (22)$$

where $\eta_{\mathbf{F}}$ is a threshold for “non-orthogonality” and $\|\cdot\|_F$ denotes the Frobenius norm.

The graph \mathcal{C} has an edge between the vertex k and vertex k' for all UE-pairs (k, k') in conflict. We consider two options for the assignment of pilots and clusters, fixed and dynamic. With the “fixed assignment” scheme, pilots and clusters are assigned to each UE $k \in [K]$ and kept fixed for all time slots. With the dynamic “pilot reassignment” scheme, clusters are fixed based on the LSFCs, but pilot allocation is carried out in each time slot after making the active user selection. Of course, it is expected that by reassigning pilots to the active users on each slot, better throughput rate performance can be achieved at the cost of a higher control signaling overhead. In contrast, the fixed assignment requires less control signaling overhead. While a precise quantitative analysis of the signaling overhead is out of the scope of this paper, it is nevertheless interesting to compare the two approaches in terms of the achieved user throughput rate.

A. Fixed Pilots and Clusters

Based on the conflict definition, we propose the following fixed pilot assignment and cluster formation scheme:

- 1) When a UE k joins the system, it connects to a maximum of \mathcal{C}_{\max} RUs with the largest LSFCs, provided that $\beta_{\ell,k} \geq \frac{\eta}{M\text{SNR}}$, forming the set \mathcal{C}_k .⁶
- 2) Each RU $\ell \in \mathcal{C}_k$ considers all pilot indices $p = [\tau_p]$. If user k is given pilot p , the set of UEs $k' \neq k$ conflicting with k is given by $\mathcal{C}_k(p) = \{\bigcup_{\ell \in \mathcal{C}_k} \mathcal{C}_{\ell,k}(p)\}$, where

$$\mathcal{C}_{\ell,k}(p) = \{k' \in \mathcal{U}_{\ell} : p_{k'} = p, \|\mathbf{F}_{\ell,k}^H \mathbf{F}_{\ell,k'}\|_F > \eta_{\mathbf{F}}\}. \quad (23)$$

In fact, these are all the users having at least one RU in common with UE k , and aligned channel subspaces in the sense of condition (22).

⁶Notice that the maximum beamforming gain of an RU array with M antennas is equal to M . Hence, this condition imposes that the SNR at UE k for the signal from RU ℓ with best-case beamforming gain is $M\beta_{\ell,k}\text{SNR} \geq \eta$, for some suitably chosen association threshold η .

- 3) Then, UE k is assigned the pilot $p_k = \arg \min_{p \in [\tau_p]} |\mathcal{C}_k(p)|$ (if the minimizer is not unique, an arbitrary choice in the minimizing set is made).

Letting for simplicity of notation $\bar{R}_k \triangleq r_k^* P_k(r_k^*)$, and defining a binary vector $\mathbf{x} \in \{0, 1\}^K$ such that the k -th entry of \mathbf{x} , i.e., x_k , is equal to 1 if $k \in \mathcal{A}(t)$ and 0 if $k \notin \mathcal{A}(t)$, the WSRM problem (17) subject to the conflict graph reduces to the linear integer program

$$\begin{aligned} & \underset{\mathbf{x}}{\text{maximize}} && \sum_{k \in [K]} Q_k(t) \bar{R}_k x_k \\ & \text{subject to} && \sum_{k \in [K]} x_k \leq K_{\text{act}}, \\ & && x_k \in \{0, 1\}, \\ & && x_k + x_{k'} \leq 1, \quad \forall (k, k') \in \mathcal{E}_c. \end{aligned} \tag{24}$$

Problem (24) can be efficiently computed using standard solvers (e.g., Gurobi or Matlab), even for fairly large systems.

B. Pilot Reassignment Scheme

As for the fixed assignment scheme, each UE k connects to a maximum of C_{\max} RUs with the largest LSFCs, provided that $\beta_{\ell,k} \geq \frac{\eta}{M \text{SNR}}$, forming the set \mathcal{C}_k for all time slots. The pilots are reassigned only to the set of active users on each time slot. However, in this case we have a classical ‘‘chicken and egg problem’’: on one hand, the set of active users must be determined in order to assign the pilots; on the other hand, the determination of the active user set depends on the pilot assignment. Our pragmatic solution consists of first running an active user pre-selection by solving the unconstrained WSRM problem, then assign pilots on the pre-selected users and determine the conflict graph, and finally solve the WSRM problem with conflict graph constraint on the restricted set of pre-selected users. For some $\tilde{K} \geq K_{\text{act}}$, the user pre-selection finds the set of \tilde{K} users maximizing (17) without conflict constraints, i.e., it solves

$$\begin{aligned} & \underset{\mathbf{x}}{\text{maximize}} && \sum_{k \in [K]} Q_k(t) \bar{R}_k x_k \\ & \text{subject to} && \sum_{k \in [K]} x_k \leq \tilde{K}, \\ & && x_k \in \{0, 1\}. \end{aligned} \tag{25}$$

The solution of (25) is immediate and consists of sorting the users in decreasing order of the product $Q_k(t) \bar{R}_k$ and selecting the top \tilde{K} sorted users. We denote such set as $\tilde{\mathcal{A}}(t)$. Then, following steps 2) and 3) of the fixed pilots scheme, pilots are assigned to the users $k \in \tilde{\mathcal{A}}(t)$ and the corresponding conflict graph $\mathcal{C}(\tilde{\mathcal{A}}(t), \mathcal{E}_c)$ is constructed. Finally, the set of active users

$\mathcal{A}(t) \subseteq \tilde{\mathcal{A}}(t)$ is the solution of

$$\begin{aligned}
& \underset{\mathbf{x}}{\text{maximize}} && \sum_{k \in \tilde{\mathcal{A}}(t)} Q_k(t) \bar{R}_k x_k \\
& \text{subject to} && \sum_{k \in \tilde{\mathcal{A}}(t)} x_k \leq K_{\text{act}}, \\
& && x_k \in \{0, 1\}, \forall k \in \tilde{\mathcal{A}}(t), \\
& && x_k = 0, \forall k \notin \tilde{\mathcal{A}}(t), \\
& && x_k + x_{k'} \leq 1, \forall (k, k') \in \mathcal{E}_{\text{c}}.
\end{aligned} \tag{26}$$

C. Proportional Fairness and Hard Fairness Scheduling

As fairness criteria in this paper we consider the very well-known PF and HF, implemented using the general Lyapunov DPP framework by selecting the appropriate network utility functions in (13). In case of PF scheduling (PFS), the network utility function is given by $g(\mathbf{a}) = \sum_{k \in [K]} \log a_k$. The corresponding solution of (16) is given by [27]

$$a_k = \min \left\{ \frac{V}{Q_k(t)}, A_{\text{max}} \right\}. \tag{27}$$

In case of HF scheduling (HFS), the network utility function is given by $g(\mathbf{a}) = \min_{k \in [K]} a_k$ and the corresponding solution to (16) is given by [27]

$$a_k = \begin{cases} A_{\text{max}}, & \text{if } V > \sum_{k \in [K]} Q_k(t), \\ 0, & \text{else.} \end{cases} \tag{28}$$

D. Mutual Information Statistics

In order to compute the instantaneous rate r_k^* according to (14), the mutual information CDF $P_k(r)$ defined in (9) is needed. Unfortunately, a closed-form expression for this CDF is intractable for the system at hand. Hence, we propose an adaptive approach where each user k accumulates samples of the instantaneous mutual information in a sliding window of N past time slots where the user is active.⁷ Based on Assumption A2 and the strong law of large numbers, the empirical CDF of $\mathcal{I}_k(\mathbb{V}_k(t), \mathbb{H}(t))$ constructed from the N samples converges to the true CDF as $N \rightarrow \infty$, and thus is a suitable approximation to compute a meaningful r_k^* with (14).⁸ In

⁷In practice, this can be done at the network infrastructure side, and the rate allocation decision can be communicated together with the scheduling decision to each user through the control information in each scheduling slot, as currently specified in the 3GPP 5G NR standard [5].

⁸As in [22], the allocated rates are initialized by a ‘‘start-up’’ phase consisting of N_{init} time slots. In each of the N_{init} time slots K_{act} out of the K UEs are randomly selected considering the conflict graph to be active. In practice, a user joining the system would start with a very conservative rate and progressively ‘‘ramp up’’ the value of r_k until the maximum of the product in (14) is achieved. Actual practical algorithms for rate scheduling work on averaged local statistics along these lines.

stationary conditions, the instantaneous mutual information distribution is independent of the slot time t . In practice, with moderate user mobility, the statistics change slowly over time. Although not investigated in this paper, the proposed method can track non-stationary (slowly varying) statistics and in fact it is very reminiscent of practical rate allocation schemes based on some time-averaged “channel quality indicator” (the role of which, in our case, is represented by the instantaneous mutual information CDF).

V. NUMERICAL RESULTS

We consider a cell-free network spanning an area of $A = 200 \times 200\text{m}^2$ with a torus topology to avoid boundary effects, containing $L = 20$ RUs, each with $M = 10$ antennas. A bandwidth of $W = 60$ MHz and noise power spectral density of $N_0 = -174$ dBm/Hz is assumed. For cluster formation we have chosen SNR threshold $\eta = 1$ and maximum cluster size $\mathcal{C}_{\max} = 7$. The LSFC statistics follow the 3GPP urban microcell street canyon pathloss model from [40, Table 7.4.1-1], which differentiates between UEs in line-of-sight (LOS) and non-LOS (NLOS). The probability of LOS is distance-dependent and given in [40, Table 7.4.2-1]. A log-normal Gaussian random variable with different parameters for LOS and NLOS is added to the deterministic distance dependent term to account for shadow fading. The UL energy per symbol is chosen such that $\bar{\beta}MSNR = 1$ (i.e., 0 dB), when the expected LSFC $\bar{\beta}$ is calculated for the considered statistics at distance $2.5d_L$, where $d_L = \sqrt{\frac{A}{\pi L}}$ is the radius of a disk of area equal to A/L . This leads to a certain level of overlap of the RUs’ coverage areas considering the RU-UE association threshold, such that each UE is likely to be associated to several RUs. The UEs are randomly dropped in the network area, while the RUs are placed on a 4×5 rectangular grid. For the rate adaptation scheme we run an initialization phase with $N_{\text{init}} = 500$ and construct for each user the instantaneous mutual information empirical CDF with $N = 100$ samples. We use RBs of dimension $T = 200$ symbols and UL pilots of dimension $\tau_p = 20$, yielding a SE penalty factor of $(1 - \frac{\tau_p}{T}) = 0.9$.

For the spatial correlation between the channel antenna coefficients, we consider a simple directional channel model defined as follows. Consider the angular support $\Theta_{\ell,k} = [\theta_{\ell,k} - \Delta/2, \theta_{\ell,k} + \Delta/2]$ centered at angle $\theta_{\ell,k}$ of the LOS between RU ℓ and UE k (with respect to the RU boresight direction), with angular spread Δ . Let \mathbf{F} denote the $M \times M$ unitary DFT matrix with (m, n) -elements $[\mathbf{F}]_{m,n} = \frac{e^{-j\frac{2\pi}{M}mn}}{\sqrt{M}}$ for $m, n = 0, 1, \dots, M - 1$, and consider the angular support set $\mathcal{S}_{\ell,k} \subseteq \{0, \dots, M - 1\}$ obtained according to the single ring local scattering

model [32], where $\mathcal{S}_{\ell,k}$ contains the DFT quantized angles (multiples of $2\pi/M$) falling inside an interval of length $\Delta = \pi/8$ placed symmetrically around the direction joining UE k and RU ℓ . Then, the channel between RU ℓ and UE k on RB f in slot t is $\mathbf{h}_{\ell,k}(t, f) = \sqrt{\frac{\beta_{\ell,k}M}{|\mathcal{S}_{\ell,k}|}} \mathbf{F}_{\ell,k} \boldsymbol{\nu}_{\ell,k}(t, f)$, where using a MATLAB-like notation $\mathbf{F}_{\ell,k} \triangleq \mathbf{F}(:, \mathcal{S}_{\ell,k})$ denotes the tall unitary matrix obtained by selecting the columns of \mathbf{F} corresponding to the index set $\mathcal{S}_{\ell,k}$,⁹ and $\boldsymbol{\nu}_{\ell,k}(t, f)$ is an $|\mathcal{S}_{\ell,k}| \times 1$ i.i.d. Gaussian vector with components $\sim \mathcal{CN}(0, 1)$. The corresponding covariance matrix is $\Sigma_{\ell,k} = \frac{\beta_{\ell,k}M}{|\mathcal{S}_{\ell,k}|} \mathbf{F}_{\ell,k} \mathbf{F}_{\ell,k}^H$. For the definition of the conflict graph (see (22)) we chose the “non-orthogonality” threshold $\eta_{\mathbf{F}} = 0$. Hence, the “non-orthogonality” condition $\|\mathbf{F}_{\ell,k}^H \mathbf{F}_{\ell,k'}\|_F > 0$ can be stated equivalently as $|\mathcal{S}_{\ell,k} \cap \mathcal{S}_{\ell,k'}| > 0$. The parameters of the scheduling policy are chosen as $V = 5,000$ and $A_{\max} = 100$.

In our simulations, we considered a total number of $K_{\text{tot}} = 10,000$ users, which is representative of a dense area such as a sports stadium (see motivation in Section I) to evaluate the described methods, i.e., a network where each frequency domain RB consists of 12 subcarriers with subcarrier spacing of 60 kHz, such that the bandwidth of each RB is $W_{\text{RB}} = 720$ kHz. We divide the system bandwidth into $\lfloor W/(FW_{\text{RB}}) \rfloor$ “subchannels” in frequency, each spanning F RBs. The K_{tot} users are distributed among the different subchannels, such that on each subchannel $K = K_{\text{tot}} \frac{FW_{\text{RB}}}{W}$ users shall be served. Out of the K users though, only a fraction $K_{\text{act}} \approx LM/2$ users are scheduled simultaneously in order to operate the network at a reasonable user load. Hence, by increasing F , the number of subchannels decreases and the number of users per subchannel increases. This means that the users are scheduled less frequently, but when they are served, they transmit at higher rate (in bit/s) since the subchannel bandwidth also grows with F . In addition, larger F yields larger frequency diversity, i.e., the CDF of the instantaneous mutual information “concentrates” due to the averaging in the frequency domain (see (3) and (7)). Since different values of F yield different subchannel bandwidths, in order to compare the performance for different F , we need to consider the actual per-user throughput rates in bit/s, obtained by multiplying the throughput rate in bit/s/Hz by the subchannel bandwidth, i.e., $\tilde{\mu}_k := \bar{\mu}_k \times FW_{\text{RB}}$. In the considered system, the number of users per subchannel with $F = 1$ is given by $K(F = 1) = K_{\text{tot}} \frac{W_{\text{RB}}}{W} = 120$. Then, for $F > 1$, the number of users per subchannel

⁹Note that for uniform linear arrays (ULAs) and uniform planar arrays (UPAs), as widely used in today’s massive MIMO implementations, the channel covariance matrix is Toeplitz (for ULA) or Block-Toeplitz (for UPA), and that large Toeplitz and block-Toeplitz matrices are approximately diagonalized by DFTs on the columns and on the rows (see [32] for a precise statement based on Szegő’s theorem).

is given by $K(F) = F \times K(F = 1)$.

In our results, we set $K_{\text{act}} = 70 \approx \frac{LM}{2}$ UEs per time slot, and $\tilde{K} = 80$ for the reassignment scheme. We identified this user density regime empirically as a good choice for typical network layouts and operating conditions considering the UL pilot dimension $\tau_p = 20$. We first evaluate the proposed schemes for a narrowband system with $F = 1$ RB. Then, we consider the effect of higher frequency diversity $F = \{5, 10\}$.

A. Utility Optimization

We consider HFS and PFS with the *fixed pilot* and *pilot reassignment* schemes, respectively. The proposed NUM-based scheduling approach is compared to a few “baseline” schemes. In particular, we have considered random selection, round-robin scheduling, and max-sum-rate scheduling.¹⁰ Random selection picks at each scheduling round K_{act} out of K UEs per time slot, independent of the previous scheduling decisions. Round-robin scheduling sorts the UEs by their index and schedule them in lexicographic order, such that at scheduling slot $t = 1, 2, 3, \dots$ the active user set is $\{t, t + 1, \dots, t + K_{\text{act}}\}$ with indices repeated periodically modulo K . The max-sum-rate scheduler selects in each time slot the K_{act} UEs to maximize the sum expected service rate. This is equivalent to fixing the virtual queues in (17) such that $Q_k(t) = 1, \forall k, t$. Fig. 3 shows the per-user throughput CDF with $F = 1$ for PFS, HFS, and the three baseline schedulers. We notice that the max-sum-rate scheduler results in a very unfair throughput rate distribution, with a large number of UEs with zero throughput (see the jump at $\tilde{\mu} = 0$ of the corresponding CDF). The PFS performs generally better than round robin and random scheduling. As expected, HFS equalizes the throughput rates across all UEs (the corresponding CDF is very close to a step function), and clearly yields a large improvement of the minimum rate with respect to PFS, while significantly reducing the maximum rates. Also, Fig. 3 compares the throughput CDF of PFS and HFS with fixed pilots and pilot reassignment, for $F = 1$. We notice that for both HFS and PFS the degradation incurred by fixed pilots with respect to the more complex pilot reassignment scheme is very moderate. This indicates that although K_{act} is significantly smaller than K , allocating UL pilots to all users independently of the scheduling decision, and performing the WSRM under the proposed conflict graph constraint, is indeed an attractive approach.

¹⁰Note that for the comparison of PFS and HFS with these baseline schedulers, we use the pilot reassignment scheme.

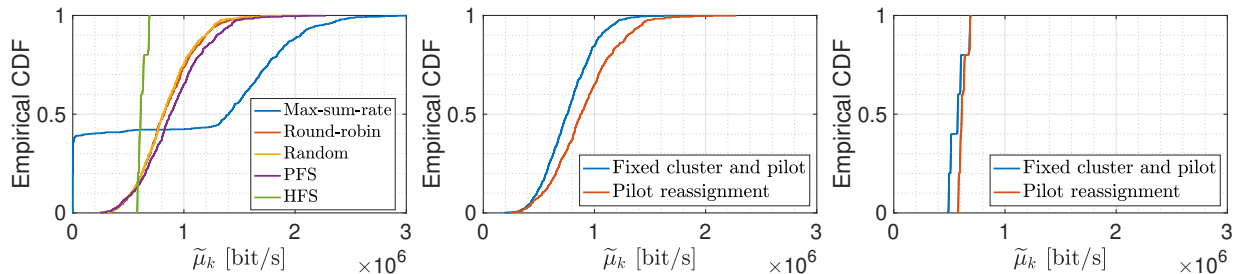


Fig. 3: The empirical CDF of the user throughput for PFS, HFS with pilot reassignment and the baseline schedulers (left). The empirical CDF of the user throughput for PFS (middle) and HFS (right) with fixed pilots and pilot reassignment.

B. Effect of the frequency diversity

Here we wish to assess the effect of increasing the frequency diversity by forming wider band subchannels with $F = \{5, 10\}$ RBs. We compare all systems under pilot reassignment. Fig. 4 shows the hardening of the instantaneous mutual information with increased frequency diversity order. In fact, the empirical CDF of the mutual information is less and less spread as F increases. This allows a more aggressive instantaneous rate allocation in the active slots. As a result (see Fig. 4), the user throughput rates in a system with $F = \{5, 10\}$ can be significantly increased compared to $F = 1$ for both PFS and HFS. This is also evidenced in Fig. 5, showing the geometric mean of the user throughputs under PFS, and the minimum user throughput under HFS. Notice that the former is directly related to the PFS objective function, since obviously $\left(\prod_{k=1}^K \tilde{\mu}_k\right)^{\frac{1}{K}} = \exp\left(\frac{1}{K}\left(\sum_{k=1}^K \log \tilde{\mu}_k\right)\right)$.

We also observe that the improvement from $F = 1$ to $F = 5$ is quite significant, while further increasing the frequency diversity to $F = 10$ yields a smaller performance gain, especially for HFS. This indicates a sort of saturation of the benefit provided by frequency diversity. As a matter of fact, since the number of users per subchannel $K(F)$ increases linearly with F , the scheduler must solve a larger WSRM problem for larger F . Hence, it is advisable to choose a moderate value of F that yields good frequency diversity gain but not a too complex scheduler.

C. Downlink Scheduling

Although in the paper we have mainly considered the UL for the sake of exposition, the same approach can be applied to the DL. Fig. 6 shows the UL/DL results for PFS and HFS, respectively, in the case of $F = 1$ and pilot reassignment, where the DL precoding vectors are identical to the UL detection vectors and uniform power allocation over all DL data streams is used, such that the total transmit power for UL and DL is identical, as explained previously.

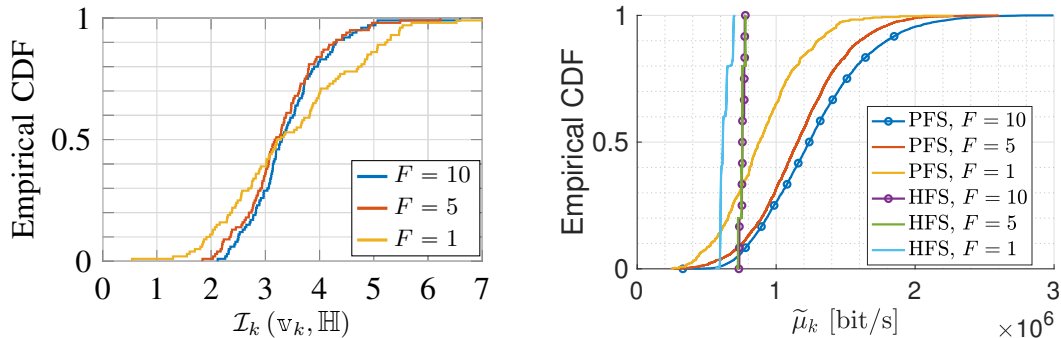


Fig. 4: The empirical CDF of $\mathcal{I}_k(\mathbb{v}_k, \mathbb{H})$ from $N = 100$ samples for a given typical user k in the center of the coverage area (left). The empirical CDF of the user throughput for PFS/HFS with $F = \{1, 5, 10\}$ using the pilot reassignment scheme (right).

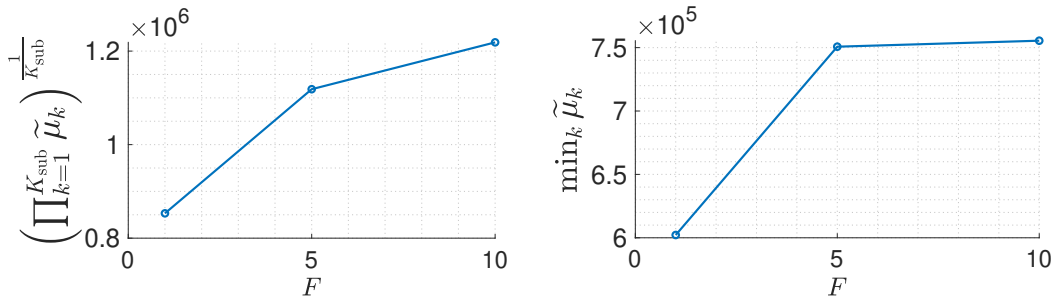


Fig. 5: The geometric mean of the user throughput under PFS (left) and the minimum throughput under HFS (right).

We notice that a similar user throughput is achieved in both cases, confirming the approximate duality results of our previous work [35]. Note that in the case of practical relevance of an imbalance in UL and DL traffic demands, a different number of time slots can be allocated to the UL and DL to meet the respective demand. Therefore, while our results show *balanced* UL and DL throughput distributions, it is clear that by unequal slot allocation one can adapt UL and DL to the actual traffic demand.

VI. CONCLUSIONS

In this work, we considered a user-centric cell-free massive MIMO network with a total number of users much larger than the optimal user load. In order to serve all users in the network with a fair distribution of throughput rates, we proposed a dynamic scheduling scheme based on Network Utility Maximization via the Lyapunov DPP approach. While the approach is quite standard, we have addressed several issues that are specific of the system at hand and represent the main novelty of this work. In particular, we considered the problem of pilot and cluster assignment, which can be fixed for all users, or dependent on the scheduling decision (reassignment). The key component of the dynamic scheduler is a novel conflict-graph constrained WSRM problem to be solved at each scheduling round, in the form of an integer linear program. Also, we

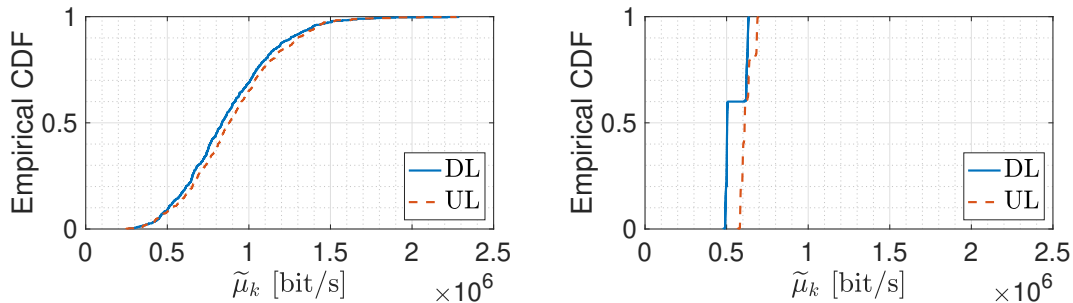


Fig. 6: The empirical CDF of the DL and UL user throughput for PFS (left) and HFS (right). In both cases $F = 1$.

considered the problem of instantaneous rate allocation in the information outage regime, based on the empirical CDF of the instantaneous mutual information that each UE can accumulate on a window of past time slots. This is very different from the standard works on cell-free massive MIMO, that consider ergodic rates and users continuously active on a (virtually infinite) sequence of fading states. In our case, block by block coding/decoding is dictated by the fact that users are scheduled on generally non-consecutive slots, and coding across slots would result in excessive decoding delay, incompatible with the low latency requirement of 5G systems. The use of information outage rates also illuminated the role of frequency diversity. For a given total number of users in the system and a total system bandwidth, allocating wider subchannels yields larger frequency diversity order, but also more users per subchannel. This means that each user is active for a smaller fraction of time, but when active it transmits at higher rates (in bit/s). We have verified that a moderate amount of frequency diversity is indeed beneficial for the user throughput. However, this benefit tends to saturate and since larger subband channels involve a higher complexity in the scheduler (namely, a larger size of the integer program to solve the WSRM problem at each scheduling round), it is advisable to carefully dimension the subchannel bandwidth in order to achieve a good tradeoff between throughput performance and scheduler complexity.

Overall, we have demonstrated the effectiveness of the proposed approach by considering a system with 10,000 users in $0.2 \times 0.2 \text{ km}^2$, a total bandwidth of 60 MHz and 200 infrastructure antennas (20 RUs with 10 antennas each). Under PFS with $F = 5$ the system achieves a geometric mean throughput rate per user of approximately 1.1 Mb/s (see Fig. 5). This corresponds to a total rate (sum over all users) of 11 Gb/s over 60 MHz, i.e., a total spectral efficiency of 183.3 bit/s/Hz per $0.2 \times 0.2 \text{ km}^2$ or, equivalently, 4582.5 bit/s/Hz per km^2 . We conclude that such system is capable of providing an excellent mean throughput rate with fairness among a large population of users, and it is therefore a very attractive solution to serve extremely dense localized areas,

such as sport stadiums, train stations, shopping malls, and similar.

APPENDIX A

PROOF OF THEOREM 1

For the proof of Theorem 1, we use the Lyapunov drift approach. The Lyapunov function defined on \mathbb{R}_+^K is given by $\mathcal{L}(\mathbf{Q}) = \frac{1}{2} \sum_{k=1}^K Q_k^2$ with the corresponding one-step Lyapunov drift

$$\Delta(\mathbf{Q}(t)) = \mathbb{E}[\mathcal{L}(\mathbf{Q}(t+1)) - \mathcal{L}(\mathbf{Q}(t)) | \mathbf{Q}(t)]. \quad (29)$$

Further, we use (18) and write

$$\begin{aligned} Q_k(t+1)^2 &= (\max\{Q_k(t) - \mu_k(t), 0\} + A_k(t))^2 \\ &\leq [Q_k(t) - \mu_k(t)]^2 + A_k^2(t) + 2A_k(t) \max\{Q_k(t) - \mu_k(t), 0\} \\ &= Q_k^2(t) + \mu_k^2(t) - 2Q_k(t)\mu_k(t) + A_k^2(t) + 2A_k(t) \max\{Q_k(t) - \mu_k(t), 0\} \\ &\leq Q_k^2(t) + \mu_k^2(t) + A_k^2(t) - 2Q_k(t) [\mu_k(t) - A_k(t)]. \end{aligned}$$

Summing with respect to k and applying the conditional expectation $\mathbb{E}[\cdot | \mathbf{Q}(t)]$, we arrive at

$$\Delta \mathbf{Q}(t) \leq \frac{1}{2} \sum_{k=1}^K \mathbb{E} [\mu_k^2(t) + A_k^2(t) | \mathbf{Q}(t)] - \sum_{k=1}^K Q_k(t) \mathbb{E} [\mu_k(t) - A_k(t) | \mathbf{Q}(t)]. \quad (30)$$

In addition, we need the following Lemma to prove Theorem 1.

Lemma 2. *Let the service rates $\{\mu_k(t)\}$ be obtained by the scheduler $\hat{\gamma}$. Then, for any $\bar{\boldsymbol{\mu}} \in \mathcal{R}$, we have $\sum_{k=1}^K Q_k(t) \mathbb{E} [\mu_k(t) | \mathbf{Q}(t)] \geq \sum_{k=1}^K Q_k(t) \bar{\mu}_k$.*

Proof: Notice that \mathcal{R} is a convex compact region in \mathbb{R}_+^K . For any fixed non-negative weight vector \mathbf{Q} , the maximum of the linear function $\sum_{k=1}^K Q_k r_k$, where $\mathbf{r} \in \mathcal{R}$, is achieved by some $\boldsymbol{\gamma} \in \Gamma$. We let $\boldsymbol{\Omega}(t)$ denote the mutual information statistics available in time slot t used to compute (14). Hence, for any $\bar{\boldsymbol{\mu}} \in \mathcal{R}$ and weight vector $\mathbf{Q}(t)$, there exists $\boldsymbol{\gamma} \in \Gamma$ such that

$$\begin{aligned} \sum_{k=1}^K Q_k(t) \bar{\mu}_k &= \sum_{k=1}^K Q_k(t) \mathbb{E} [\mu_k(\mathbb{H}(t), \boldsymbol{\gamma}(\boldsymbol{\Omega}(t)))] \\ &= \sum_{k=1}^K Q_k(t) \mathbb{E} \left[\mathbb{E} [\mu_k(\mathbb{H}(t), \boldsymbol{\gamma}(\boldsymbol{\Omega}(t))) | \boldsymbol{\Omega}(t), \boldsymbol{\gamma}] \right] \\ &\leq \mathbb{E} \left[\max_{\boldsymbol{\mathcal{A}}(t)} \sum_{k=1}^K Q_k(t) \mathbb{E} [\mu_k(\mathbb{H}(t), \boldsymbol{\mathcal{A}}(t)) | \boldsymbol{\Omega}(t)] \middle| \mathbf{Q}(t) \right] \\ &= \sum_{k=1}^K Q_k(t) \mathbb{E} \left[\mathbb{E} [\mu_k(\mathbb{H}(t), \hat{\boldsymbol{\gamma}}(\boldsymbol{\Omega}(t))) | \boldsymbol{\Omega}(t)] \middle| \mathbf{Q}(t) \right]. \end{aligned} \quad (31)$$

Since we assumed that the service rates $\mu_k(t)$ are obtained by applying the policy $\hat{\gamma}$, then by definition $\mathbb{E}\left[\mathbb{E}[\mu_k(\mathbb{H}(t), \hat{\gamma}(\Omega(t))) | \Omega(t)] | \mathbf{Q}(t)\right] = \mathbb{E}[\mu_k(t) | \mathbf{Q}(t)]$, and the Lemma is proved. ■

Proof of Theorem 1. We define $\bar{\mathbf{A}}(t) = \frac{1}{t} \sum_{\tau=0}^{t-1} \mathbb{E}[\mathbf{A}(\tau)]$ and $\bar{\boldsymbol{\mu}}(t) = \frac{1}{t} \sum_{\tau=0}^{t-1} \mathbb{E}[\boldsymbol{\mu}(\tau)]$, where $\mathbf{A}(\tau)$ and $\boldsymbol{\mu}(\tau)$ are the virtual arrival process and the service rate vector induced by $\hat{\gamma}$. From [27], we know that

$$\frac{1}{t} \sum_{\tau=0}^{t-1} \mathbb{E}[\mathbf{A}(\tau)] \leq \frac{1}{t} \sum_{\tau=0}^{t-1} \mathbb{E}[\boldsymbol{\mu}(\tau)] + \frac{\mathbb{E}[\mathbf{Q}(t)]}{t}. \quad (32)$$

We will use the following preliminary fact, whose proof uses (32) and the fact that strong stability and uniformly bounded arrival processes imply mean-rate stability (i.e., $\mathbb{E}[\mathbf{Q}(t)/t \rightarrow \mathbf{0}]$) [25].

Fact 1. *We assume that the queues $\mathbf{Q}(t)$ are strongly stable and that there is a finite upper bound A_{\max} on arrivals for all t . If $g(\cdot)$ is a continuous and componentwise non-decreasing function, then*

$$\liminf_{t \rightarrow \infty} g(\bar{\mathbf{A}}(t)) \leq \liminf_{t \rightarrow \infty} g(\bar{\boldsymbol{\mu}}(t)), \quad (33)$$

$$\limsup_{t \rightarrow \infty} g(\bar{\mathbf{A}}(t)) \leq g(\bar{\boldsymbol{\mu}}^*(A_{\max})). \quad (34)$$

◇

We further observe that $\mathbb{E}[\mu_{k^*}^2(t)] \leq \mathbb{E}\left[\left(\frac{1}{F} \sum_{f=1}^F \log\left(1 + \frac{|\mathbb{h}_{k^*}(t,f)|^2}{\text{SNR}^{-1}}\right)\right)^2\right]$, where the latter is the maximum achievable instantaneous rate of UE k^* , given by $\arg \max_{k \in [K]} \frac{1}{F} \sum_{f=1}^F \log\left(1 + \frac{|\mathbb{h}_k(t,f)|^2}{\text{SNR}^{-1}}\right)$, under perfect CSI and as if it was alone in the system. It follows that

$$\frac{1}{2} \sum_{k=1}^K \mathbb{E}[\mu_k^2(t) + A_k^2(t) | \mathbf{Q}(t)] \leq \frac{K}{2} \left(A_{\max}^2 + \mathbb{E}\left[\left(\frac{1}{F} \sum_{f=1}^F \log\left(1 + \frac{|\mathbb{h}_{k^*}(t,f)|^2}{\text{SNR}^{-1}}\right)\right)^2\right] \right) \triangleq C < \infty. \quad (35)$$

From (30), (35) and Lemma 2, we know that

$$\Delta(\mathbf{Q}(t)) \leq C - \sum_{k=1}^K Q_k(t) \bar{\mu}_k + \sum_{k=1}^K Q_k(t) \mathbb{E}[A_k(t) | \mathbf{Q}(t)], \quad (36)$$

where $\Delta(\mathbf{Q}(t))$ is the Lyapunov drift defined in (29), C is given in (35) and $\bar{\boldsymbol{\mu}} = [\bar{\mu}_1, \dots, \bar{\mu}_K]^\top$ is any rate vector in \mathcal{R} . Following the technique in [25], [26], we subtract a term related to the utility function from both sides of (36), which yields

$$\Delta(\mathbf{Q}(t)) - V \mathbb{E}[g(\mathbf{A}(t)) | \mathbf{Q}(t)] \leq C - \sum_{k=1}^K Q_k(t) \bar{\mu}_k + \mathbb{E}\left[\sum_{k=1}^K Q_k(t) A_k(t) - V g(\mathbf{A}(t)) | \mathbf{Q}(t)\right]. \quad (37)$$

We note that $\hat{\gamma}$ is defined in (16) such that it minimizes the right hand side over all vectors \mathbf{a} that satisfy $0 \leq a_k \leq A_{\max}$ for all k . Now, let \mathbf{z} be any vector in \mathcal{R} that satisfies $0 \leq z_k \leq A_{\max}$

for all k . Then

$$\Delta(\mathbf{Q}(t)) - V\mathbb{E}[g(\mathbf{A}(t))|\mathbf{Q}(t)] \leq C - \sum_{k=1}^K Q_k(t)\bar{\mu}_k + \sum_{k=1}^K Q_k(t)z_k(t) - Vg(\mathbf{z}). \quad (38)$$

Taking expectations of both sides of the above inequality and using the law of iterated expectations yields

$$\mathbb{E}[\mathcal{L}(\mathbf{Q}(t+1))] - \mathbb{E}[\mathcal{L}(\mathbf{Q}(t))] - V\mathbb{E}[g(\mathbf{A}(t))] \leq C - \sum_{k=1}^K \mathbb{E}[Q_k(t)](\bar{\mu}_k - z_k) - Vg(\mathbf{z}). \quad (39)$$

We assume $\mathbf{Q}(t) = \mathbf{0}$ for simplicity. The above inequality holds for all t . Summing over $\tau \in \{0, \dots, t-1\}$, dividing by t , rearranging terms, and using the non-negativity of $\mathcal{L}(\cdot)$ we have

$$\frac{1}{t} \sum_{\tau=0}^{t-1} \sum_{k=1}^K \mathbb{E}[Q_k(\tau)](\bar{\mu}_k - z_k) \leq C + Vg(\bar{\mathbf{A}}(t)) - Vg(\mathbf{z}), \quad (40)$$

where we used Jensen's inequality in the concave function $g(\cdot)$. The above inequality holds for all t , all $\bar{\boldsymbol{\mu}} \in \mathcal{R}$, and all $\mathbf{z} \in \mathcal{R}$ such that $0 \leq z_k \leq A_{\max}$ for all k . Parts (a) and (b) of Theorem 1 are proven by plugging different values into (40). We first prove part (b).

Proof of part (b). Take any point $\tilde{\mathbf{z}} \in \mathcal{R}$ such that $\tilde{\mathbf{z}} = [\tilde{z}_1 \dots \tilde{z}_K]^\top$ and $0 \leq \tilde{z}_k \leq A_{\max}$ for all k . Choose $\bar{\boldsymbol{\mu}} = \tilde{\mathbf{z}}$ and $\mathbf{z} = \beta\tilde{\mathbf{z}}$, for any $\beta \in [0, 1]$. Then, from (40), we have

$$\frac{1}{t} \sum_{\tau=0}^{t-1} \sum_{k=1}^K \tilde{z}_k \mathbb{E}[Q_k(\tau)] \leq \frac{C + Vg(\bar{\mathbf{A}}(t)) - Vg(\beta\tilde{\mathbf{z}})}{1 - \beta}. \quad (41)$$

Now, we first prove that the queues are strongly stable and then, using Fact 1, we obtain part (b) of Theorem 1. Notice that $g(\bar{\mathbf{A}}(t)) \leq g(\mathbf{A}_{\max})$, where \mathbf{A}_{\max} is a vector with each entry equal to A_{\max} . Using this bound in (41) and taking a lim sup yields

$$\limsup_{t \rightarrow \infty} \frac{1}{t} \sum_{\tau=0}^{t-1} \sum_{k=1}^K \tilde{z}_k \mathbb{E}[Q_k(t)] \leq \frac{C + Vg(\mathbf{A}_{\max}) - Vg(\beta\tilde{\mathbf{z}})}{1 - \beta}. \quad (42)$$

By assumption, there exists at least one point $\mathbf{r} \in \mathcal{R}$ that has all positive entries and such that $g(\frac{\mathbf{r}}{2}) > -\infty$. Choosing $\beta = \frac{1}{2}$ and $\tilde{\mathbf{z}} = \mathbf{r}$, it follows that the right-hand side of (42) is finite and hence all queues are strongly stable.

Because of strong stability and since the arrival processes are bounded by $A_{\max} < \infty$, we can apply inequality (34) of Fact 1 to the right-hand side of (41) after taking a lim sup and obtain the result of part (b).

Proof of part (a). We obtain $g(\bar{\mathbf{A}}(t)) \geq g(\bar{\boldsymbol{\mu}}^*(A_{\max})) - \frac{C}{V}$ by plugging $\bar{\boldsymbol{\mu}} = \mathbf{z} = \bar{\boldsymbol{\mu}}^*(A_{\max})$ into (40). By taking lim inf and using (33) of Fact 1, we obtain the result of (a).

REFERENCES

- [1] G. Caire and S. Shamai (Shitz), "On the achievable throughput of a multiantenna Gaussian broadcast channel," *IEEE Trans. on Inform. Theory*, vol. 49, no. 7, pp. 1691–1706, July 2003.

- [2] P. Viswanath and D. N. C. Tse, "Sum capacity of the vector Gaussian broadcast channel and uplink-downlink duality," *IEEE Trans. on Inform. Theory*, vol. 49, no. 8, pp. 1912–1921, Aug. 2003.
- [3] H. Weingarten, Y. Steinberg, and S. Shamai (Shitz), "The capacity region of the Gaussian multiple-input multiple-output broadcast channel," *IEEE Trans. on Inform. Theory*, vol. 52, no. 9, pp. 3936–3964, Sept. 2006.
- [4] G. Caire, N. Jindal, M. Kobayashi, and N. Ravindran, "Multiuser MIMO achievable rates with downlink training and channel state feedback," *IEEE Trans. on Inform. Theory*, vol. 56, no. 6, pp. 2845–2866, June 2010.
- [5] 3GPP, "NR; Physical channels and modulation," 3GPP Tech. Spec. 38.211, 04 2022, Version 17.1.0.
- [6] T. L. Marzetta, E. G. Larsson, H. Yang, and H. Q. Ngo, *Fundamentals of Massive MIMO*. Cambridge University Press, 2016.
- [7] Ö. T. Demir, E. Björnson, L. Sanguinetti *et al.*, "Foundations of User-Centric Cell-Free Massive MIMO," *Foundations and Trends® in Signal Processing*, vol. 14, no. 3-4, pp. 162–472, 2021.
- [8] E. Khorov, A. Kiryanov, A. Lyakhov, and G. Bianchi, "A tutorial on IEEE 802.11 ax high efficiency WLANs," *IEEE Communications Surveys & Tutorials*, vol. 21, no. 1, pp. 197–216, Sept. 2018.
- [9] Q. Qu, B. Li, M. Yang, Z. Yan, A. Yang, D.-J. Deng, and K.-C. Chen, "Survey and performance evaluation of the upcoming next generation WLANs standard-IEEE 802.11 ax," *Mobile Networks and Applications*, vol. 24, no. 5, pp. 1461–1474, Oct. 2019.
- [10] T. L. Marzetta, "Noncooperative cellular wireless with unlimited numbers of base station antennas," *IEEE Trans. on Wireless Comm.*, vol. 9, no. 11, pp. 3590–3600, 2010.
- [11] J. Hoydis, S. Ten Brink, and M. Debbah, "Massive mimo in the ul/dl of cellular networks: How many antennas do we need?" *IEEE Journal on selected Areas in Communications*, vol. 31, no. 2, pp. 160–171, 2013.
- [12] H. Huh, G. Caire, H. C. Papadopoulos, and S. A. Ramprasad, "Achieving "Massive MIMO" Spectral Efficiency with a Not-so-Large Number of Antennas," *IEEE Trans. on Wireless Commun.*, vol. 11, no. 9, pp. 3226–3239, 2012.
- [13] H. Q. Ngo, A. Ashikhmin, H. Yang, E. G. Larsson, and T. L. Marzetta, "Cell-Free Massive MIMO Versus Small Cells," *IEEE Trans. on Wireless Commun.*, vol. 16, no. 3, pp. 1834–1850, 2017.
- [14] E. Nayeri, A. Ashikhmin, T. L. Marzetta, H. Yang, and B. D. Rao, "Precoding and Power Optimization in Cell-Free Massive MIMO Systems," *IEEE Trans. on Wireless Commun.*, vol. 16, no. 7, pp. 4445–4459, 2017.
- [15] E. Björnson and L. Sanguinetti, "Scalable Cell-Free Massive MIMO Systems," *IEEE Trans. on Comm.*, vol. 68, no. 7, pp. 4247–4261, 2020.
- [16] L. Miretti, E. Björnson, and D. Gesbert, "Team MMSE Precoding With Applications to Cell-Free Massive MIMO," *IEEE Trans. on Wireless Commun.*, vol. 21, no. 8, pp. 6242–6255, 2022.
- [17] F. Götsch, N. Osawa, T. Ohseki, K. Yamazaki, and G. Caire, "Subspace-Based Pilot Decontamination in User-Centric Scalable Cell-Free Wireless Networks," *IEEE Trans. on Wireless Commun.*, vol. 22, no. 6, pp. 4117–4131, 2023.
- [18] 3GPP, "NR; NR and NG-RAN Overall description; Stage-2," 3GPP Tech. Spec. 38.300, 05 2022, Version 17.0.0.
- [19] S. Chen, J. Zhang, E. Björnson, and B. Ai, "Improving Fairness for Cell-Free Massive MIMO Through Interference-Aware Massive Access," *IEEE Transactions on Vehicular Technology*, pp. 1–6, 2022.
- [20] ITU-R, "Minimum requirements related to technical performance for IMT-2020 radio interface(s)," Report ITU-R M.2410-0, 11 2017.
- [21] G. Durisi, T. Koch, and P. Popovski, "Toward Massive, Ultrareliable, and Low-Latency Wireless Communication With Short Packets," *Proceedings of the IEEE*, vol. 104, no. 9, pp. 1711–1726, 2016.
- [22] F. Götsch, N. Osawa, T. Ohseki, Y. Amano, I. Kanno, K. Yamazaki, and G. Caire, "Fairness Scheduling in Dense User-Centric Cell-Free Massive MIMO Networks," in *2022 56th Asilomar Conference on Signals, Systems, and Computers*, 2022, pp. 733–737.

- [23] A. Forenza, S. Perlman, F. Saibi, M. Di Dio, R. van der Laan, and G. Caire, "Achieving large multiplexing gain in distributed antenna systems via cooperation with pCell technology," in *2015 49th Asilomar Conference on Signals, Systems and Computers*, 2015, pp. 286–293.
- [24] E. Biglieri, J. Proakis, and S. Shamai, "Fading channels: Information-theoretic and communications aspects," *IEEE transactions on information theory*, vol. 44, no. 6, pp. 2619–2692, 1998.
- [25] L. Georgiadis, M. J. Neely, L. Tassiulas *et al.*, "Resource allocation and cross-layer control in wireless networks," *Foundations and Trends® in Networking*, vol. 1, no. 1, pp. 1–144, 2006.
- [26] M. J. Neely, E. Modiano, and C.-P. Li, "Fairness and optimal stochastic control for heterogeneous networks," *IEEE/ACM Transactions On Networking*, vol. 16, no. 2, pp. 396–409, 2008.
- [27] H. Shirani-Mehr, G. Caire, and M. J. Neely, "MIMO downlink scheduling with non-perfect channel state knowledge," *IEEE Transactions on Communications*, vol. 58, no. 7, pp. 2055–2066, 2010.
- [28] J. Mo and J. Walrand, "Fair end-to-end window-based congestion control," *IEEE/ACM Transactions on networking*, vol. 8, no. 5, pp. 556–567, 2000.
- [29] Z. Chen and E. Björnson, "Channel Hardening and Favorable Propagation in Cell-Free Massive MIMO With Stochastic Geometry," *IEEE Transactions on Communications*, vol. 66, no. 11, pp. 5205–5219, 2018.
- [30] H. Huh, A. M. Tulino, and G. Caire, "Network MIMO with linear zero-forcing beamforming: Large system analysis, impact of channel estimation, and reduced-complexity scheduling," *IEEE Trans. on Inform. Theory*, vol. 58, no. 5, pp. 2911–2934, 2012.
- [31] D. Bethanabhotla, O. Y. Bursalioglu, H. C. Papadopoulos, and G. Caire, "Optimal user-cell association for massive MIMO wireless networks," *IEEE Trans. on Wireless Commun.*, vol. 15, no. 3, pp. 1835–1850, 2015.
- [32] A. Adhikary, J. Nam, J.-Y. Ahn, and G. Caire, "Joint Spatial Division and Multiplexing—The Large-Scale Array Regime," *IEEE Trans. on Inform. Theory*, vol. 59, no. 10, pp. 6441–6463, 2013.
- [33] F. Ye, J. Li, P. Zhu, D. Wang, H. Wu, and X. You, "Spectral Efficiency Analysis of Cell-Free Distributed Massive MIMO Systems With Imperfect Covariance Matrix," *IEEE Systems Journal*, vol. 16, no. 4, pp. 5402–5412, 2022.
- [34] F. Göttsch, N. Osawa, T. Ohseki, K. Yamazaki, and G. Caire, "The Impact of Subspace-Based Pilot Decontamination in User-Centric Scalable Cell-Free Wireless Networks," in *2021 IEEE 22nd International Workshop on Signal Processing Advances in Wireless Communications (SPAWC)*, 2021, pp. 406–410.
- [35] —, "Uplink-Downlink Duality and Precoding Strategies with Partial CSI in Cell-Free Wireless Networks," in *2022 IEEE Wireless Communications and Networking Conference (WCNC)*, 2022, pp. 614–619.
- [36] Y. Polyanskiy, H. V. Poor, and S. Verdú, "Channel Coding Rate in the Finite Blocklength Regime," *IEEE Trans. on Inform. Theory*, vol. 56, no. 5, pp. 2307–2359, 2010.
- [37] W. Yang, G. Durisi, T. Koch, and Y. Polyanskiy, "Quasi-Static Multiple-Antenna Fading Channels at Finite Blocklength," *IEEE Trans. on Inform. Theory*, vol. 60, no. 7, pp. 4232–4265, 2014.
- [38] 3GPP, "NR; Physical layer procedures for data," 3GPP Tech. Spec. 38.214, 05 2022, Version 17.1.0.
- [39] 3GPP, "NR; Requirements for support of radio resource management," 3GPP Tech. Spec. 38.133, 10 2022, Version 17.7.0.
- [40] 3GPP, "Study on channel model for frequencies from 0.5 to 100 GHz (Release 16)," 3GPP Tech. Spec. 38.901, 12 2019, Version 16.1.0.